ChemCatChem

Research Article
doi.org/10.1002/cctc.202200700

Chemistry Europe
European Chemical Societies Publishing

www.chemcatchem.org

Nickel Nanoparticles for Liquid Phase Toluene Oxidation – Phenomenon, Opportunities and Challenges

Adél Anna Ádám,[a, b] Szilveszter Ziegenheim,[a, b] Ádám Papp,[a, b] Márton Szabados,[a, b] Zoltán Kónya,[c, d] Ákos Kukovecz,[c] and Gábor Varga*[e]

Effective oxidative transformation of toluene into valuable products was achieved under solvent-free reaction conditions with as-prepared nickel nanoparticles as heterogeneous catalysts in liquid phase. The crystalline structure and size of the as-prepared nanoparticles were confirmed by X-ray diffractometry (XRD) and dynamic light scattering (DLS). The catalytic implications of the different crystalline forms (face-centred cubic: fcc; hexagonal close-packed: hcp) of these nanocatalysts were investigated. The product selectivity of toluene oxidation was found to vary depending on the crystalline forms of the catalyst. Fcc nanocatalysts showed remarkable chemoselectivity (83 mol%) for the product benzyl alcohol and were readily reusable. In contrast, the hcp Ni phase showed reasonable reusability but lower chemoselectivity (29 mol%) compared to its fcc counterpart. Moreover, the simple organic solvents used had a remarkable effect on the crystal structure and phase purity of the Ni nanocrystals, which also affected the catalytic process.

Introduction

In recent years, the catalytic applications of 3d transition metal nanoparticles, composites and foams were rapidly growing in popularity because of their advantages such as low cost, abundant accessible redox active sites and really good mass transfer ability.[1–6] These properties and their suitable catalytic activities made them viable candidates to replace the expensive platinum group metals used as conventional catalysts in many organic transformations.[7–10] Among these, supported and unsupported nickel catalysts have one of the most versatile catalytic potentials, covering not only cross-coupling reactions but also redox transformations in liquid or gas phase.[11–19] Recently, nickel species, especially nickel foams have been tested in toluene/VOC oxidations, but, usually as metallic substrates or modular catalysts under gas phase conditions.[20,21] On one hand, it was found that no significant activity could be attributed to the nickel metal. On the other hand, there was no significant oxidation (either complete or partial) on the metallic surfaces. As actual catalysts, nickel nanoparticles (Ni NPs) have well-known popularity in liquid phase redox coupling reactions in conventional solvents such as toluene, alcohols or DMSO.[17,19,22] In our previous work, the desired transformations were indeed feasible in the presence of nickel nanocatalysts. In contrast to the studies reported, a significant but yet unknown rearrangement in the crystal phase of the nickel NPs was observed in parallel with their notable deactivation.[22] By now, it became evident that the efficiency of nickel catalysis through nanoparticles highly depends on factors such as crystalline size, porosity or electronic structure as well as surface area, etc.[23–26] Unexpectedly, the face-centred cubic (fcc) crystalline form of Ni NPs was used for the catalysis of the above chemical reactions with almost exclusive selectivity. This fact may be ascribed to the metastable feature of the hexagonal closed-packed (hcp) crystalline form of Ni NPs.[27]

While fcc Ni NPs have been prepared *via* numerous synthesis strategies, controlling their morphology, crystal shape and crystallite size, the preparation of phase pure, size-controlled hcp Ni NPs still remains a challenge.[27–29] Moreover, it became evident that direct transformation of fcc Ni NPs into its hcp counterpart can occur over 350 °C because of high stacking-fault energy (SFE) of fcc Ni NPs (450 mJ m^{-2}).[28,30] The different crystalline phases of Ni NPs display significant differences in their physico-chemical properties, enabling their versatile utilisations in many different fields of material science.[31–34] These differences considering the crystal phases of Ni NPs are largely untested in catalytic liquid phase trans-

[a] Dr. A. A. Ádám, Dr. S. Ziegenheim, Á. Papp, Dr. M. Szabados
Department of Organic Chemistry
University of Szeged
Dóm tér 8
Szeged, H-6720 (Hungary)
[b] Dr. A. A. Ádám, Dr. S. Ziegenheim, Á. Papp, Dr. M. Szabados
Material and Solution Structure Research Group
Institute of Chemistry
University of Szeged
Aradi Vértanúk tere 1
Szeged, H-6720 (Hungary)
[c] Prof. Z. Kónya, Prof. Á. Kukovecz
Department of Applied and Environmental Chemistry
University of Szeged
Rerrich B. tér 1
Szeged, H-6720 (Hungary)
[d] Prof. Z. Kónya
MTA-SZTE Reaction Kinetics and Surface Chemistry Research Group
Rerrich B tér 1
Szeged, H-6720 (Hungary)
[e] Dr. G. Varga
Department of Physical Chemistry and Materials Science
University of Szeged
Rerrich Béla sq. 1.
Szeged, H-6720 (Hungary)
E-mail: gabor.varga5@chem.u-szeged.hu

formations. In sharp contrast, a well-defined structure-activity relationship has been identified in a few examples in gas phases reactions.[33]

This study focuses on the crystalline phase-activity-selectivity-stability relationships in the catalytic, liquid phase oxidation of the toluene promoted by nickel nanocrystals. The above detailed trends and caveats motivated us to study and determine the role of phase transition/phase purity of nickel nanocrystals as catalysts during the oxidation reaction. Nickel nanocrystals were found to behave as active, selective and more or less reusable catalysts for the liquid phase toluene oxidation. It was observed that massive changes in the crystalline phases of Ni NPs could be induced by a simple solvent treatment at reflux temperature. It was also demonstrated that the presence of the different crystalline phases and their absolute ratios can noticeably affect not only the catalytic activity but also the selectivity and reusability of the Ni NPs.

Results and Discussion

Solvent compatibility of the fcc Ni NPs

As mentioned in the introduction, significant decrease in the catalytic activity of the fcc Ni nanocatalyst was observed in our previous work, which was attributed to an unknown phase transition of the Ni NPs. To prove that this observation was not due to an unlikely solvent effect, the phase stability of the fcc Ni nanocatalysts was first studied during treatment in various, commercially available organic solvents (DMSO, DMF, ethanol, toluene) at reflux temperature and in the absence of other chemicals. For comparisons, Ni in hcp crystalline phase and a physically mixed fcc/hcp composite were also produced.

The starting material was a highly crystalline, phase pure solid, XRD patterns of which were analogous to that of fcc crystalline phase metal Ni NPs (Figure 1A) (JCPDS#04-0850). The hcp form and the mixed phase exhibited Bragg reflections that could be assigned to Miller planes corresponding to the unit cell dimensions of hcp metal Ni (JCPDS#45-1027), allowing discrimination between these and fcc Ni. The particle size distributions presented that heterodisperse nanoparticles were produced in all cases (Figure 1C). The XRD patterns of the obtained products after the solvent treatment, filtration and drying can be found in Figure 1B. Surprisingly, considerable effects of the solvents on the crystalline phase of the fcc Ni NPs were seen in all cases. By using DMSO treatment, the Ni NPs were completely transformed into a phase pure NiS (JCPDS#12-0041), while the application of DMF or ethanol allowed the partial occurrence of the thermodynamically hindered fcc-hcp phase transition. Additionally, a second NiO phase (JCPDS#78-0643) was also formed in DMF. In toluene, the fcc Ni crystalline phase remained the main fraction, however, with the appearance of a second phase with amorphous features. Furthermore, in all cases there was a significant decrease in the crystallinity of the Ni NPs as a result of the solvent treatment. Since dissolution of the solids was not observed, a solid-solid transformation

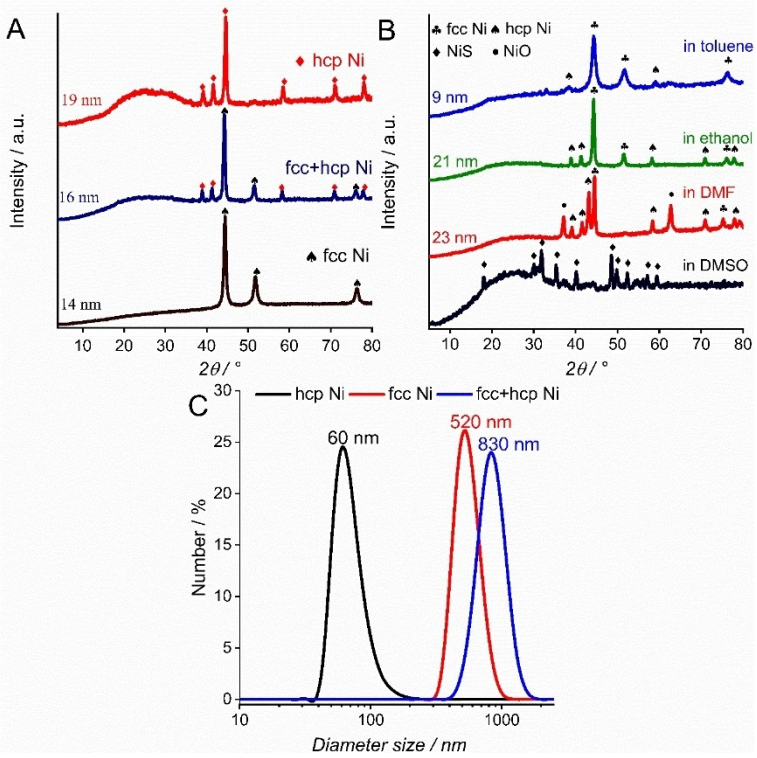

Figure 1. XRD patterns of the as-prepared nickel nanostructures (A) and solvent treated fcc nanocrystals (B). Crystal size distributions of the as-prepared nickel nanocrystals (C).

must be suggested in all cases. Beside the transformation of the crystalline phase, significant changes in the primary particle sizes were also noticed (Figure 1). These findings could be clearly associated with the appearance of the hcp or amorphous phase. In order, to compare the catalytic performance of the different crystalline phases of the Ni NPs in toluene oxidation, the solvent effect described above had to be avoided, which is why the further tests were carried out under solvent-free reaction conditions in pure toluene.

Toluene oxidation on Ni NPs

The initial step of our study was the optimization of the reaction conditions for toluene oxidation on fcc Ni nanocatalysts (Figure 2). Initially, a reaction time of 60 minutes was used in toluene at reflux temperature applying 50 mg catalyst. The desired oxidation was not feasible in the absence of any catalyst when peroxides or oxygen were used as oxidants. In contrast, when the oxidant phenyliodine(III) diacetate (PIDA) was used, a considerable product yield (~30 mol%) was observed, however, with pure selectivity for the benzyl benzoate product. This was very odd, as the Tishchenko reaction, which can produce this non-commercial product, cannot be carried out under non-catalytic conditions. We suspected that hypervalent iodine – which could be derived from the oxidant – acted as the actual catalyst.[35,36]

The application of phenyliodine(III) diacetate oxidant resulted in a notable product yield in the Ni catalysed reactions, while other oxidants (O_2, H_2O_2, *etc.*) proved to be useless. Compared to catalyst-free conditions, the main difference was in product yield (100 mol%), while a remarkable shift in product selectivity from phenyl benzoate to benzoic acid (100 mol%) was also observed. There was no detectable change in toluene conversions due to the change in total volume of oxidant (Figure 3A). In contrast, by decreasing the load of the oxidant,

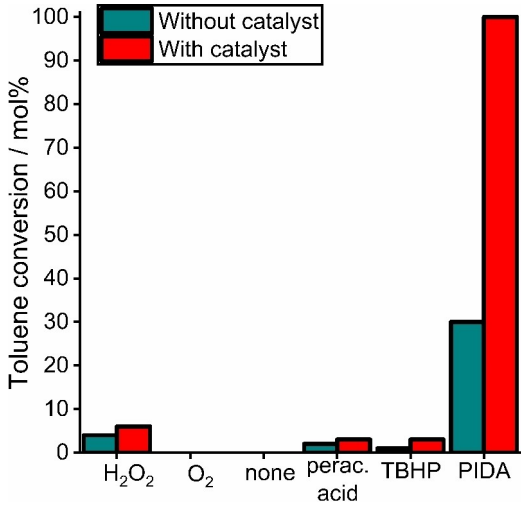

Figure 2. The effect of the quality of the oxidants in the toluene oxidation reaction (see Scheme 1. Reaction conditions: 5 ml toluene, 0.5 ml water (additive), 50 mg catalyst, reflux temperature for 60 minutes.

the product selectivity shifted toward the more valuable chemicals such as benzaldehyde and benzyl alcohol (up to 83 mol%). Although the product selectivity and the reaction rate really depend on the loading and the quality of the oxidant, the toluene oxidation is promoted by nickel (NPs) without the addition of other metals/metal ions (Pd, Pt *etc.*), in contrast to the results obtained under gas phase conditions.

The key role of the Ni NPs as actual catalysts was highlighted by the systematic decrease of the nickel feed (Figure 3B), which led to a striking decrease in the product yields, albeit, with unchanged selectivities. Finally, it was found that the application of any reaction temperature other than the reflux temperature led to a marked decrease in the product yield of benzyl alcohol (Figure 3C).

With the optimised nickel catalysis in hand, the performance of the different Ni crystalline phases was tested under the same reaction conditions as described above. Total conversion of the toluene was achieved by means of nickel catalysis, regardless of the crystalline phase of the solids (Figure 4). However, significant differences in product selectivities were observed depending on the quality of the catalysts. In particular, excellent benzyl alcohol selectivity (83 mol%) of fcc Ni NPs was found, while the hcp Ni did not show significant chemoselectivity, but gave products in reasonable amounts. The catalyst of mixed crystalline phase appeared to be less alcohol selective than that of fcc phase, but showed better chemoselectivity than hcp nickel. In view of this, the investigation of a possible phase transition under these reaction conditions became increasingly important.

The observed differences in the selectivity of the catalysts may be due to the slightly different reaction mechanisms. One of the conceivable, however, envisioned reaction mechanisms is described below. Considering the literature data on toluene oxidation over transition metal nanocatalysts, the key factor found was that the nanocatalysts were able to adsorb molecular oxygen with a side-on orientation on their surfaces and subsequently cleave the O–O bond by multi-electron transfer from the nanoparticles to the oxygen.[37,38] These probably led to the formation of an electronic core-shell structure of the nanoparticles and the negatively charged shell can promote charge transfer to the π^*-orbital of oxygen. In addition, the newly formed quasi-NiO surface may exhibit hydrophobic feature,[39] which promotes the adsorption of toluene molecules that react with oxygen species on the surface. Subsequently, the surface of the catalyst loses its hydrophobic property and desorption of the (hydrophobic) products occurs. Previously, it was found that the catalytic activity of the nanoparticles in oxidation reactions is really dependent on the oxophilicity of the transition metals.[40] Since Ni nanoparticles are highly oxophilic,[41] this feature should be considered as the key for the remarkable activity of Ni NPs. However, the aforementioned laterally aligned adsorption of molecular oxygen would only occur at the distinguished positions of the edge sites. Comparing fcc Ni nanocatalysts with hcp Ni nanocatalysts or mixed-phase catalysts described above, these edge sites must differ in both quality and quantity based on the structural evidences.[42] This is crucial because oxophilic surfaces are even capable of stabilizing hydroxyl and/or oxo-hydroxyl species,[43]

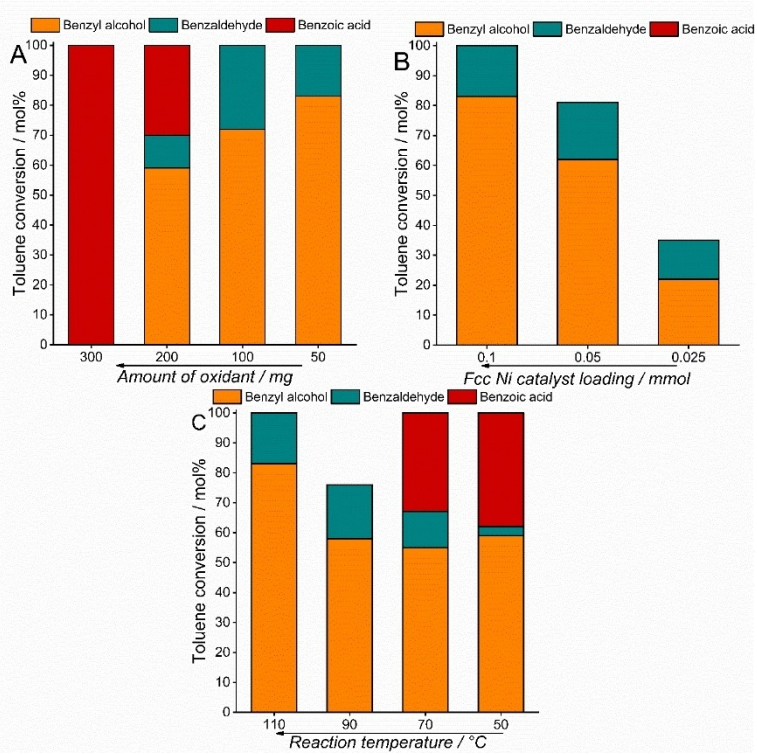

Figure 3. Conversions of toluene as a function of the oxidant supply (A), fcc Ni catalyst loading (B) as well as reaction temperature (C). Reaction conditions: 5 ml toluene, 0.5 ml water (additive), 6 mg fcc Ni catalyst (A, C), 50 mg PIDA (B, C), reflux temperature (A, B) for 60 minutes.

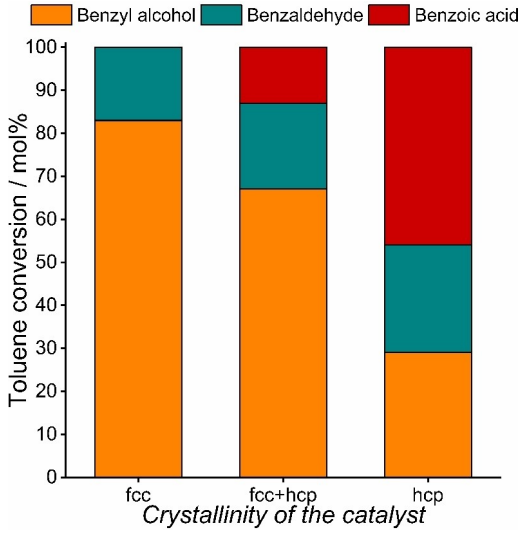

Figure 4. Catalytic ability of the different crystalline phases of nickel nanoparticles in toluene oxidation. Reaction conditions: 5 ml toluene, 0.5 ml water (additive), 6 mg catalyst, 50 mg PIDA, reflux temperature for 60 minutes.

leading to significant variations in product distribution. This could be the decisive factor affecting the selectivity of the toluene oxidation over various nickel nanocatalysts detailed.

After the first use, the nickel catalysts were separated from the reaction mixtures by filtration, washed completely with ethanol and reused after XRD measurements (Figure 5). The results confirmed that both the fcc and mixed phase NPs recrystallised into an α-Ni(OH)$_2$/β-Ni(OH)$_2$/fcc Ni mixture, while the hcp Ni phase completely transformed into its fcc-phase counterpart. It should be noted that an amorphous phase was also observed in all cases.

Given the fact of the phase transformations, it seemed fairly obvious that significant differences in selectivity – at least – should occur when recycling the phase transformed nickel catalysts. On one hand, since there is no evidence of a decrease in toluene conversion, one should not assume significant leaching or poisoning. It also became clear that the catalytic behaviour of Ni catalysts is largely dependent on the quality of the original crystalline phase. As Figure 6 shows, no notable changes were observed in either product yields or product selectivities, regardless of whether the catalysts were derived from hcp or mixed phase Ni NPs. It was also evident that repeated recirculation of these composites did not result in any change in their crystalline phase or catalytic ability. In contrast, the sample originated from fcc Ni NPs showed substantially different selectivity compared to the initial selectivity of the starting sample, so much so that the actual ratio of benzyl alcohol and benzoic acid detected was almost completely balanced after the third run. These findings could be related to the presence of different active centres on the surfaces of the catalysts.

To test this hypothesis, the initial TOF values of the phase transformed hcp and fcc and the original fcc catalysts as well as

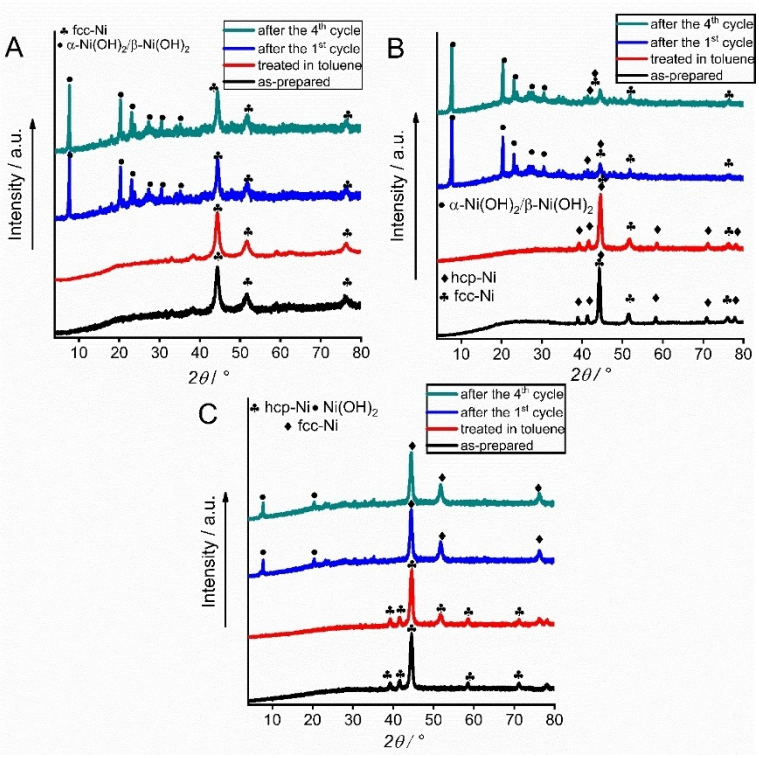

Figure 5. XRD patterns of as-prepared, toluene treated and reused fcc (A), fcc + hcp physically mixed (B) and hcp (C) Ni catalysts.

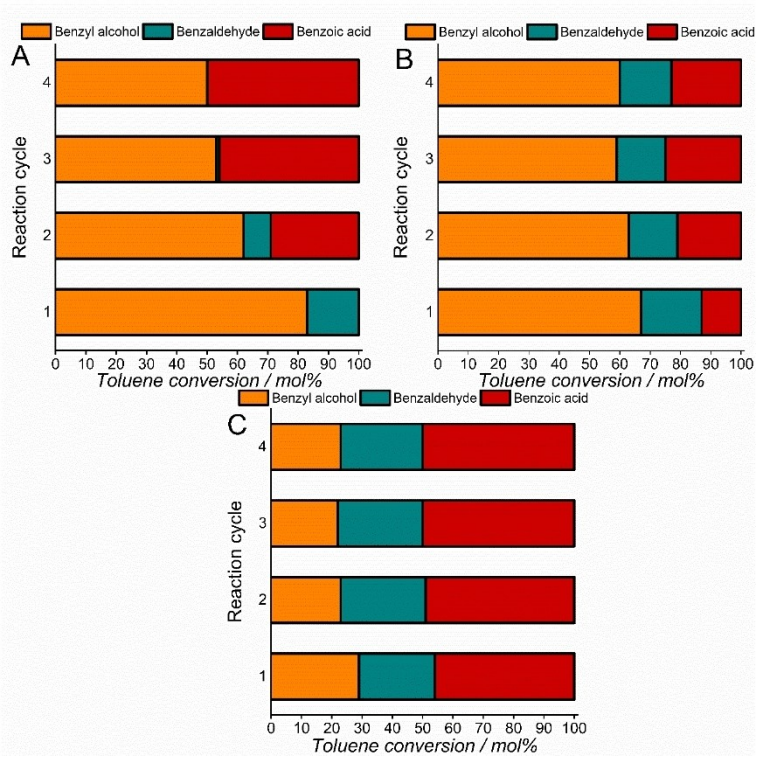

Figure 6. Reusability of fcc (A), fcc + hcp physically mixed (B) and hcp (C) Ni catalysts. Reaction conditions: 5 ml toluene, 0.5 ml water (additive), 6 mg catalyst, 50 mg PIDA, reflux temperature for 60 minutes.

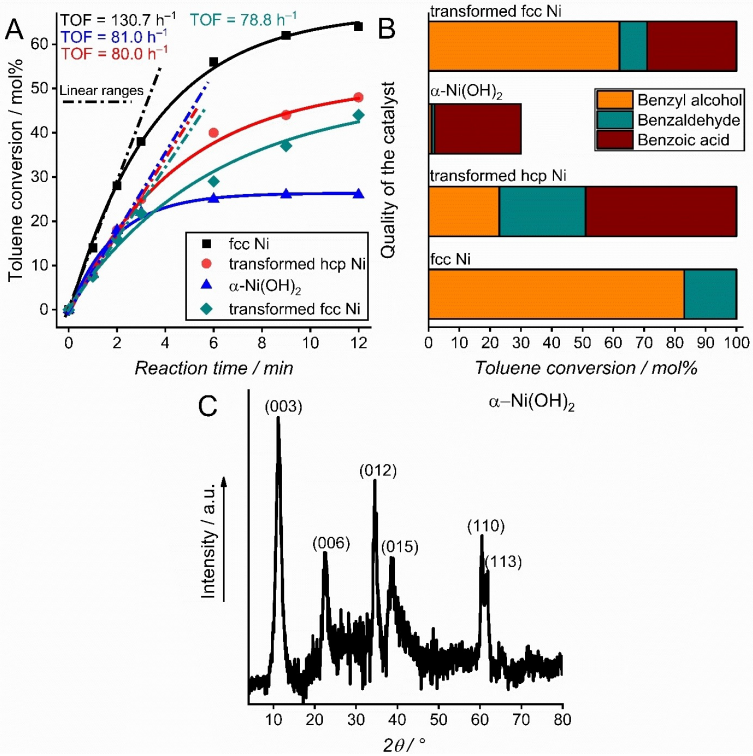

Figure 7. Conversions of toluene as the function of time in the toluene oxidation reaction (A). Reaction conditions: 5 ml toluene, 0.5 ml water (additive), 6 mg catalyst, 50 mg PIDA, reflux temperature. The effect of the quality of the catalysts in the toluene oxidation (B). Reaction conditions: 5 ml toluene, 0.5 ml water (additive), 6 mg catalyst, 50 mg PIDA, reflux temperature for 60 minutes. XRD patterns of the as-prepared α-Ni(OH)$_2$ (C).

pure α-Ni(OH)$_2$ prepared for comparison (Figure 7C, PDF#38-0715), were determined and compared (Figure 7A). It became clear that there were significant differences in the TOF values of the untreated and the transformed fcc nickel catalysts, indicating the diversity of the active sites on their surfaces. Besides, almost the same initial TOF values were obtained for the pure nickel hydroxide and the transformed hcp Ni catalyst. This finding should be regarded as proof for the main active role of the α-Ni(OH)$_2$ centres formed in-situ on the surface of the metallic nanocatalysts and dictated the catalytic activity during the reuse cycles. However, the selectivities, which were constant over time for each sample, and the maximum possible conversions achieved (Figure 7B) by the catalysts varied greatly. These differences revealed the co-catalytic feature of the metallic components of the transformed structures, which strongly influenced both the product distribution and the maximum conversion rate.

Conclusion

In conclusion, the reaction rates of toluene oxidation carried out with nickel nanocrystal catalysts were comparable to those of efficient, well-known catalysts reported previously. The catalytic markers studied revealed that nickel nanocatalysts can function adequately under solvent-free reaction conditions when the oxidant phenyliodine(III) diacetate is used. It was also clearly presented that the dosage of oxidant had a significant effect on the selectivity of the reaction while the reaction rate could be strongly influenced by changing the catalyst loading. Remarkable differences were observed in the catalytic behaviour of the different crystal phases (fcc, hcp) of the nickel nanocrystals, which in all cases allowed effective oxidation of toluene, albeit with different selectivities and reusability. Solvent-initialized, unprecedented phase transitions were observed under both the applied reaction conditions and when a simple solvent treatment was used. During the recycling of the Ni nanocatalysts, in-situ formation of composites with α-Ni(OH)$_2$ was observed, which proved to be efficient and stable catalysts for toluene oxidation.

Experimental Section

Materials

Anhydrous nickel iodide (NiI$_2$), anhydrous potassium hydroxide (KOH) pellets, N,N-dimethylformamide (DMF), dimethyl sulfoxide (DMSO), toluene, hexane, absolute ethanol and acetone were purchased from VWR International. Nickel acetate tetrahydrate, oleylamine, oleic acid, phenyliodine(III) diacetate (PIDA), benzyl-alcohol, benzoic acid and polyethylene glycol 400 (PEG 400) were purchased from Sigma-Aldrich and hydrazine monohydrate ($N_2H_4 \times H_2O$) (98 + %) was ordered from Alfa Aesar. All chemicals were used as received.

Synthesis of the fcc Ni nanoparticles

The fcc Ni NPs were synthetized by chemical reduction, based on our previous study. First, NiI_2 of 5 mmol was dissolved in 12.5 mL of absolute ethanol. Then, the potassium hydroxide (Ni^{2+}/KOH = 1/10) and hydrazine monohydrate (Ni^{2+}/KOH = 1/10) were mixed in another vessel also with 12.5 mL of absolute ethanol. The first solution was poured into the second one and the mixture was stirred at 25 °C for 4 h. The obtained slurries were filtered and washed with distilled water and absolute ethanol of 20–20 mL and then dried at 25 °C under a desiccator.

Synthesis of the hcp Ni nanoparticles

The hcp Ni nanoparticles were prepared according to Tzitzios's study with minor modifications.[44] The reaction was carried out in a two-neck flask under reflux conditions. The flask contained the mixture of 10 mL PEG 400; 0.4 g oleylamine and 0.4 g oleic acid and the temperature was raised to 120 °C. 0.124 g nickel acetate tetrahydrate was added to the vigorously stirred solution. The reaction mixture was kept at 120 °C for 30 min and then heated to the boiling point of PEG 400 for 60 min. The black precipitates sedimented overnight and were filtered, washed with 20 mL acetone as well as distilled water (30 mL). Finally, the particles were dried and stored in a desiccator under N_2 atmosphere at 60 °C.

Structural transformation of fcc Ni nanoparticles to hcp form

The structural transformation of Ni NPs was studied in DMF, DMSO, ethanol and toluene. The previously prepared fcc nanoparticles (0.2 g) were added to the appropriate solvent of 20 mL at reflux temperature. The suspension of nanoparticles was stirred for 24 h. The black precipitate was filtered and washed with distilled water as well as ethanol (30 mL). The NPs were dried and stored under desiccator as described above.

Synthesis of α-$Ni(OH)_2$

For a comparison, α-$Ni(OH)_2$ was prepared using an urea hydrolysis method reported previously.[45] Typically, $Ni(NO_3)_2 \times 6H_2O$ (0.242 g) and urea (0.278 g) were added into distilled water (2.315 g) and stirred for 30 minutes. This solution was then kept at 100 °C with constant magnetic stirring for 12 h. After a further 12 hours of maturation in the mother solution at the same temperature, the precipitates were separated by centrifugation, washed several times with water and ethanol and dried in an oven at 60–65 °C (Scheme 1.

Procedure of the catalytic toluene oxidation reaction

The catalytic oxidation of toluene as a test reaction was carried out in a 10 mL batch reactor using a hot plate with magnetic stirring. The mixture of toluene and water (5 mL/0.5 mL) was heated to 80 °C followed by the addition of solid phenyliodine(III) diacetate (PIDA) and Ni nanoparticles into the hot, vigorously stirred solution.

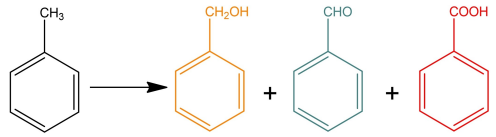

Scheme 1. Schematic reaction pathway of the catalytic toluene oxidation.

The slurry was stirred at reflux temperature (~110 °C) for 1 h. Then the solids were separated by filtration and the internal standard (n-hexane) was added to the reaction. Finally, the crude products were analysed by a gas chromatograph (GC). The GC was a Hewlett-Packard 5890 Series II instrument equipped with 50-m-long Agilent HP-1 column and a flame ionization detector. Initial turnover frequency (TOF) values were determined from the initial reaction rates as the number of molecules transformed per unit time and per surface nickel atoms.[46,47]

After the oxidation reaction, the nickel specimens were separated from the reaction mixture by filtration, washed thoroughly with water and alcohols and then reused as catalysts in subsequent cycles under the optimized reaction conditions. The structural features of the catalysts used were monitored by XRD measurements.

Methods of structural characterization

The powder X-ray diffractograms (XRD) were recorded in the range $2\theta = 4–80°$ with a Rigaku Miniflex II instrument with $4° min^{-1}$ scan speed, using CuK_α ($\lambda = 1.5418$ Å) radiation. The characteristic reflections in the normalized diffractograms were identified on the basis of JCPDS-ICDD (Joint Committee of Powder Diffraction Standards- International Centre for Diffraction Data) database. The primary particle (average crystallite) sizes of nanoparticles were calculated from the most intense (111) reflections using the Scherrer equation with a shape factor of 0.9.

The secondary particle sizes and polydispersity indices were determined by dynamic light scattering. For these measurements a Malvern NanoZS dynamic light scattering (DLS) instrument was used, operated with a 4-mW helium-neon laser light source ($\lambda =$ 633 nm) at room temperature, in backscattering mode at 173°.The nanoparticles were dispersed in the mixture of ethanol and ethylene glycol (1:2) by 1 h ultrasonic irradiation. The concentration of the light-grey semi-transparent dispersion was 0.05 g dm^{-3}.

Acknowledgements

This work was supported by the European Union and the Hungarian government through grant GINOP-2.3.2-15-2016-00013. Márton Szabados gratefully acknowledges the support of Bolyai Janos Research Fellowship (BO/00246/21/7) of the Hungarian Academy of Science and the UNKP-21-5-SZTE-560 New National Excellence Program of the Ministry for the Innovation and Technology from the Source of the National Research Development and Innovation Fund. The financial help is highly appreciated.

Conflict of Interest

The authors declare no conflict of interest.

Data Availability Statement

The data that support the findings of this study are available from the corresponding author upon reasonable request.

Keywords: fcc/hcp nickel · nanocatalysts · phenyliodine(III) diacetate oxidant · phase transition · toluene oxidation

[1] K. Wang, L. Yang, W. Zhao, L. Cao, Z. Sun, F. Zhang, *Green Chem.* **2017**, *19*, 1949–1957.
[2] K. Guo, H. Li, Z. Yu, *ACS Appl. Mater. Interfaces* **2018**, *10*, 517–525.
[3] A. R. Hajipour, F. Rezaei, Z. Khorsandi, *Green Chem.* **2017**, *19*, 1353–1361.
[4] D. Balcells, A. Nova, *ACS Catal.* **2018**, *8*, 3499–3515.
[5] S. Y. Zhao, Z. Y. Chen, N. Wei, L. Liu, Z. B. Han, *Inorg. Chem.* **2019**, *58*, 7657–7661.
[6] J. Yao, F. Dong, H. Feng, Z. Tang, *ACS Appl. Nano Mater.* **2021**, *4*, 9322–9332.
[7] C. A. Malapit, J. R. Bour, C. E. Brigham, M. S. Sanford, *Nature* **2018**, *563*, 100–104.
[8] K. Hong, M. Sajjadi, J. M. Suh, K. Zhang, M. Nasrollahzadeh, H. W. Jang, R. S. Varma, M. Shokouhimehr, *ACS Appl. Nano Mater.* **2020**, *3*, 2070–2103.
[9] X. Wang, S. Min, S. K. Das, W. Fan, K. W. Huang, Z. Lai, *J. Catal.* **2017**, *355*, 101–109.
[10] X. Chen, J. Li, Y. Wang, Y. Zhou, Q. Zhu, H. Lu, *Appl. Catal. A* **2020**, *607*, 117839:1–8.
[11] Y. Ren, H. Wei, G. Yin, L. Zhang, A. Wang, T. Zhang, *Chem. Commun.* **2017**, *53*, 1969–1972.
[12] H. Alinezhad, K. Pakzad, M. Nasrollahzadeh, *Appl. Organomet. Chem.* **2020**, *34*, 1–16.
[13] W.-M. Feng, T.-Y. Li, L.-J. Xiao, Q.-L. Zhou, *Org. Lett.* **2021**, 0–4.
[14] Y. Jin, H. Yang, C. Wang, *Org. Lett.* **2019**, *21*, 7602–7608.
[15] C. M. Farley, C. Uyeda, *Trends Chem.* **2019**, *1*, 497–509.
[16] T. Wang, Y. Zhao, H. Zhang, W. Hui, *J. CO_2 Util.* **2021**, *45*, 101417.
[17] W. Gong, C. Chen, H. Zhang, Y. Zhang, Y. Zhang, G. Wang, H. Zhao, *J. Mol. Catal.* **2017**, *429*, 51–59.
[18] G. Gao, P. Sun, Y. Li, F. Wang, Z. Zhao, Y. Qin, F. Li, *ACS Catal.* **2017**, *7*, 4927–4935.
[19] C. Jiang, Z. Shang, X. Liang, *ACS Catal.* **2015**, *5*, 4814–4818.
[20] Q. Zhang, S. Mo, B. Chen, W. Zhang, C. Huang, D. Ye, *J. Mol. Catal.* **2018**, *454*, 12–20.
[21] Y. F. Guo, D. Q. Ye, K. F. Chen, J. C. He, *Catal. Today* **2007**, *126*, 328–337.
[22] A. A. Ádám, M. Szabados, G. Varga, Á. Papp, K. Musza, Z. Kónya, Á. Kukovecz, P. Sipos, I. Pálinkó, *Nanomaterials* **2020**, *10*, 632:1–18.
[23] L. Zhang, X. Hu, *Chem. Sci.* **2020**, *11*, 10786–10791.
[24] N. Sahiner, F. Seven, *Energy* **2014**, *71*, 170–179.
[25] B. Zhu, J. Lu, S. Sakaki, *J. Catal.* **2021**, *397*, 13–26.
[26] K. W. Park, J. H. Choi, B. K. Kwon, S. A. Lee, Y. E. Sung, H. Y. Ha, S. A. Hong, H. Kim, A. Wieckowski, *J. Phys. Chem. B* **2002**, *106*, 1869–1877.
[27] E. G. C. Neiva, M. M. Oliveira, L. H. Marcolino, A. J. G. Zarbin, *J. Colloid Interface Sci.* **2016**, *468*, 34–41.
[28] A. S. Bolokang, M. J. Phasha, *Mater. Lett.* **2011**, *65*, 59–60.
[29] H. Lin, H. Lin, J. X. Liu, H. Fan, W. X. Li, *J. Phys. Chem. C* **2020**, *124*, 11005–11014.
[30] C. B. Carter, S. M. Holmes, *Philos. Mag.* **1977**, *35*, 1161–1171.
[31] Q. Shao, Y. Wang, S. Yang, K. Lu, Y. Zhang, C. Tang, J. Song, Y. Feng, L. Xiong, Y. Peng, Y. Li, H. L. Xin, X. Huang, *ACS Nano* **2018**, *12*, 11625–11631.
[32] C. Wang, Y. Wang, H. Yang, Y. Zhang, H. Zhao, Q. Wang, *Small* **2018**, *14*, 1–7.
[33] M. H. Aghaali, S. Firoozi, *Powder Technol.* **2019**, *356*, 119–128.
[34] S. Andrieu, T. Hauet, M. Gottwald, A. Rajanikanth, L. Calmels, A. M. Bataille, F. Montaigne, S. Mangin, E. Otero, P. Ohresser, P. Le Fèvre, F. Bertran, A. Resta, A. Vlad, A. Coati, Y. Garreau, *Phys. Rev. Mater.* **2018**, *2*, 064410:1–11.
[35] M. Ochiai, Y. Takeuchi, T. Katayama, T. Sueda, K. Miyamoto, *J. Am. Chem. Soc.* **2005**, *127*, 12244–12245.
[36] S. K. Alla, R. K. Kumar, P. Sadhu, T. Punniyamurthy, *Org. Lett.* **2013**, *15*, 1334–1337.
[37] A. Staykov, T. Nishimi, K. Yoshizawa, T. Ishihara, *J. Phys. Chem. C* **2012**, *116*, 15992–16000.
[38] M. Huda, K. Minamisawa, T. Tsukamoto, M. Tanabe, K. Yamamoto, *Angew. Chem. Int. Ed.* **2019**, *58*, 1002–1006; *Angew. Chem.* **2019**, *131*, 1014–1018.
[39] W. Geng, A. Hu, M. Li, *Appl. Surf. Sci.* **2012**, *263*, 821–824.
[40] F. Liu, Q. Yan, W. J. Zhou, X. S. Zhao, J. Y. Lee, *Chem. Mater.* **2006**, *18*, 4328–4335.
[41] M. Alesker, M. Page, M. Shviro, Y. Paska, G. Gershinsky, D. R. Dekel, D. Zitoun, *J. Power Sources* **2016**, *304*, 332–339.
[42] E. G. C. Neiva, M. M. Oliveira, L. H. Marcolino, A. J. G. Zarbin, *J. Colloid Interface Sci.* **2016**, *468*, 34–41.
[43] Z. Cao, Q. Chen, J. Zhang, H. Li, Y. Jiang, S. Shen, G. Fu, B. A. Lu, Z. Xie, L. Zheng, *Nat. Commun.* **2017**, *8*, 15131:1–7.
[44] V. Tzitzios, G. Basina, M. Gjoka, V. Alexandrakis, V. Georgakilas, D. Niarchos, N. Boukos, D. Petridis, *Nanotechnology* **2006**, *17*, 3750–3755.
[45] J. T. Zhang, S. Liu, G. L. Pan, G. R. Li, X. P. Gao, *J. Mater. Chem. A* **2014**, *2*, 1524–1529.
[46] M. Wolf, *RSC Adv.* **2021**, *11*, 18187–18197.
[47] M. J. Eslamibidgoli, A. Groß, M. Eikerling, *Phys. Chem. Chem. Phys.* **2017**, *19*, 22659–22669.

Manuscript received: May 31, 2022
Revised manuscript received: August 20, 2022
Accepted manuscript online: August 23, 2022
Version of record online: September 22, 2022